International Journal of Mass Spectrometry 281 (2009) 108–114

Contents lists available at ScienceDirect

International Journal of Mass Spectrometry

journal homepage: www.elsevier.com/locate/ijms

The effect of endcap electrode holes on the resonant ejection from an ion trap

Hideya Koizumi[a], William B. Whitten[a], Peter T.A. Reilly[a,*], Eiko Koizumi[b]

[a] Oak Ridge National Laboratory, Oak Ridge, TN 37831, United States
[b] Department of Mathematics, Peace College, Raleigh, NC 27604, United States

ARTICLE INFO

Article history:
Received 11 September 2008
Received in revised form
23 December 2008
Accepted 26 December 2008
Available online 4 January 2009

Keywords:
Ion trap
Resonance ejection
Endcap hole effects
Higher order field effects

ABSTRACT

The presence of endcap holes greatly influences the performance of an ion trap mass spectrometer. Optimizing the shape and size of the holes may significantly improve ion trap performance. The field contours have been numerically simulated at varying hole sizes and the potentials were numerically fitted. The presence of holes in the electrodes adds higher order negative components to the field inside the trap. The absolute values of the field components were found to increase with increasing hole size. The fitted potentials were then used to reexamine the amplitude response functions. The addition of negative higher order field components produces up to four jump points in the amplitude response function. The new jump points may produce multiple jump phenomena in forward scans as well as a jump condition in the reverse scan mode that has not previously been considered. The shape of the amplitude response function is dependent on the hole size and the amplitude of the dipole excitation waveform at constant buffer gas pressure. The shape of the function has interesting implications for the resonance ejection process. This work provides new insights into the resonance excitation process in nonlinear ion traps.

1. Introduction

It has been 12 years since Makarov [1] explained the phenomenal resolution observed in the resonant ejection mode at low scanning rates for ion traps [2–4]. He was the first to use asymptotic theory to describe the jump in the amplitude of oscillation when the ions neared resonance due to the addition of octopole components to the field induced by stretching the trap (i.e., increasing the distance between endcaps). While the addition of positive octopole components to the field by stretching the geometry qualitatively explained the reason for the jump in oscillatory amplitude near resonance, it did not fully describe the effects of the higher order fields experienced by the ions inside the trap due to the endcap electrode holes.

The effects of the holes on the fields were studied by several groups and were found to be significant [5,6]. More recently, Ding et al. [7] found that the use of a precision mesh over the exit endcap hole and a field adjusting electrode just outside the entrance endcap hole permitted excellent resolution in an un-stretched trap. Their modifications essentially nullified the higher order field components caused by the presence of the holes. This enabled a trap with an idealized electrode spacing to achieve much higher resolution than had previously been observed [8].

To date, none of the analytical approaches [1,3,9–15] account for the presence of the higher order terms caused by the presence of the holes in the endcap electrodes though they are often mentioned. Fields from outside penetrate into the trap through the endcap holes adding negative higher order components to the field. Unfortunately, adding more terms to the expansion that describes the fields inside an ion trap makes the solutions to the equations of ion motion more cumbersome, so they were generally ignored for the sake of expedience.

In this work, the higher order field components caused by stretching the trap geometry and adding endcap electrode holes have been incorporated into the amplitude response plot. The simulated potential along the *z*-axis of a 10.7% stretched ion trap was then fit to a polynomial expansion that accounted for the higher order fields induced by the endcap holes with three different diameters. The odd order terms induced by the disparate potentials outside the endcap electrodes were found to have little influence on the fields inside the trap and so they were set to zero. Even order terms up to dodecapole were used to fit the potential inside the trap. These terms were then incorporated into a model to determine the amplitude response function that has been so aptly used to describe the jump of ions when they near resonance. This work provides new insight to the ion dynamics inside nonlinear traps.

* Corresponding author at: Oak Ridge National Laboratory, Chemical Sciences Division, P.O. Box 2008, MS 6142, Oak Ridge, TN 37831, United States.
Tel.: +1 865 574 4919; fax: +1 865 574 8363.
E-mail address: ReillyPT@ornl.gov (P.T.A. Reilly).

1387-3806/$ – see front matter © 2008 Elsevier B.V. All rights reserved.
doi:10.1016/j.ijms.2008.12.018

2. Theory

In cylindrical coordinates, the potential inside a nonlinear ion trap with azimuthal symmetry can be written as

$$\Phi(\rho,\theta,t) = V_0\ \cos(\Omega t)\sum_{n=0}^{\infty}\frac{\rho^n}{r_0^n}A_nP_n(\cos\ \theta) + U_0(\rho,\theta) \tag{1}$$

where A_n is dimensionless expansion coefficient, P_n is a Legendre polynomial of order n, V_0 is the RF voltage at frequency $\Omega/(2\pi)$ applied to the ring electrode, r_0 is the radius of the trap, and the last term corresponds to the DC component. The last term was dropped for reasons described below. Converting to Cartesian coordinates, the motion of an ion within a pseudo-potential well is given by

$$m\frac{d^2r}{dt^2} + e\nabla U_{eff}(r,z) = -e\nabla U_{exc}(r,z) \tag{2}$$

where U_{eff} and U_{exc} are the time averaged pseudo-potential and excitation potential, respectively. U_{eff} is given by

$$U_{eff}(r,z) = \frac{e}{2m}\left\langle\left|\int_t \nabla\phi\ dt\right|^2\right\rangle \tag{3}$$

The above expression may be simplified by setting the radial dispersion to zero. Because we are interested in the dynamics near the endcap holes, higher order terms are included to represent the field components due to the endcap holes. The time averaged pseudo-potential along the z-axis has the following form:

$$U_{eff}(z) = \frac{e}{m\Omega^2}\left(\frac{A_2}{r_0^2}V_0\right)^2\left[z^2 + \frac{4f}{r_0^2}z^4 + \frac{3g}{r_0^4}z^6 + O(\varepsilon^7)\right] \tag{4}$$

where O represents the rest of the higher order terms. Parameters, f and g are ratios of octopole to quadrupole and dodecapole to quadrupole field strength defined as A_4/A_2 and A_6/A_2, respectively. Using the Mathieu parameter,

$$q_z = \frac{4eA_2V_0}{mr_0^2\Omega^2} \tag{5}$$

the corresponding equation of motion of an anharmonic oscillator is given by

$$\frac{d^2z}{dt^2} + \omega_0^2 z + \beta z^3 + \eta z^5 + O(z^6) = \frac{\hat{f}}{m}\cos\ \gamma t \tag{6}$$

where

$$\omega_0^2 = \frac{eq_zA_2V}{2mr_0^2} \tag{7}$$

$$\beta = \frac{8A_4\omega_0^2}{A_2r_0^2}\ \text{and} \tag{8}$$

$$\eta = \frac{9A_6\omega_0^2}{A_2r_0^4} \tag{9}$$

where ω_0 is the secular frequency and γ is the frequency applied to the endcap electrode with force, $\hat{f}$.

The odd nonlinear terms have been eliminated to simplify the equation. For a stretched trap, β is generally set positive and one or more of the higher order terms set negative to account for the field penetration of the outside through the ion trap. The solution of this equation can be found using the Lindstedt–Poincare technique [26]. This requires successively approximating the solution such that

$$x(j\text{th}) = \sum_{i=1}^{j} x_i \tag{10}$$

$$\omega(j\text{th}) = \sum_{i=1}^{j} \omega_{i-1} \tag{11}$$

where the trial function x_1 is given by

$$x_1 = z\ \cos\omega t \tag{12}$$

Extending the equation of motion only up to the 5th nonlinear term, we obtain

$$x_2 = x_4 = 0 \tag{13}$$

$$x_3 = \left(\frac{\beta z^3}{32\omega_0^2}\right)\cos 3\omega t \tag{14}$$

$$x_5 = \left(-\frac{3\beta^2z^5}{64\omega_0^2} - \frac{5z^5\eta}{16}\right)\cos 3\omega t + \left(-\frac{3\beta^2z^5}{128\omega_0^2} - \frac{z^5\eta}{16}\right)\cos 5\omega t \tag{15}$$

$$\omega_1 = \omega_3 = 0 \tag{16}$$

$$\omega_2 = \frac{3\beta z^2}{8\omega_0} \tag{17}$$

$$\omega_4 = \left(\frac{5\eta}{16\omega_0} - \frac{15\beta^2}{256\omega_0^3}\right)z^4 \tag{18}$$

The expression for the frequency shift due to the octopole component, ω_2, is in agreement with work by others [16]. The frequency shift including dodecapole fields is then given by

$$\Delta\omega = \frac{3\beta z^2}{8\omega_0} + \left(\frac{5\eta}{16\omega_0} - \frac{15\beta^2}{256\omega_0^3}\right)z^4 \tag{19}$$

The damping term as defined in Michaud et al. [17] may now be added to the equation of motion:

$$\frac{d^2z}{dt^2} + 2\lambda\frac{dz}{dt} + \omega_0^2 z + \beta z^3 + \eta z^5 + O(z^6) = \frac{\hat{f}}{m}\cos\gamma t \tag{20}$$

where the damping constant, λ, is defined using a drag coefficient model. The damping constant is related to the collision cross section and gas number density by

$$\lambda = \frac{3.01\sqrt{2kT/m_n}\sigma n m_n}{4m_i} \tag{21}$$

where m_i, m_n, k, σ, and n represent ion mass, neutral mass, Boltzmann's constant, collision cross section, and number density of the buffer gas, respectively [17].

The solution of the equation of motion up to inclusion of octopole field components is outlined in standard mechanics textbooks [16,18,19]. Defining the detune parameter as $\varepsilon = \gamma - \omega_0$, the amplitude dependent frequency of the ions can be written as $\gamma = \omega_0 + \kappa Z^2 + \varepsilon$. Recognizing that the frequency correction expressions contain only even powers of amplitude, the amplitude dependent frequency can be rewritten as

$$\gamma = \omega_0 + \sum_i \kappa_{2i}z^{2i} + \varepsilon \tag{22}$$

The following expressions for the coefficients were obtained algebraically:

$$\kappa_2 = 3\frac{A_4}{A_2}\left(\frac{1}{r_0^2}\right)\omega_0 \tag{23}$$

$$\kappa_4 = \left(\frac{45}{16}\frac{A_6}{A_2} - \frac{15A_4^2}{4A_2^2}\right)\left(\frac{1}{r_0^2}\right)^2\omega_0 \tag{24}$$

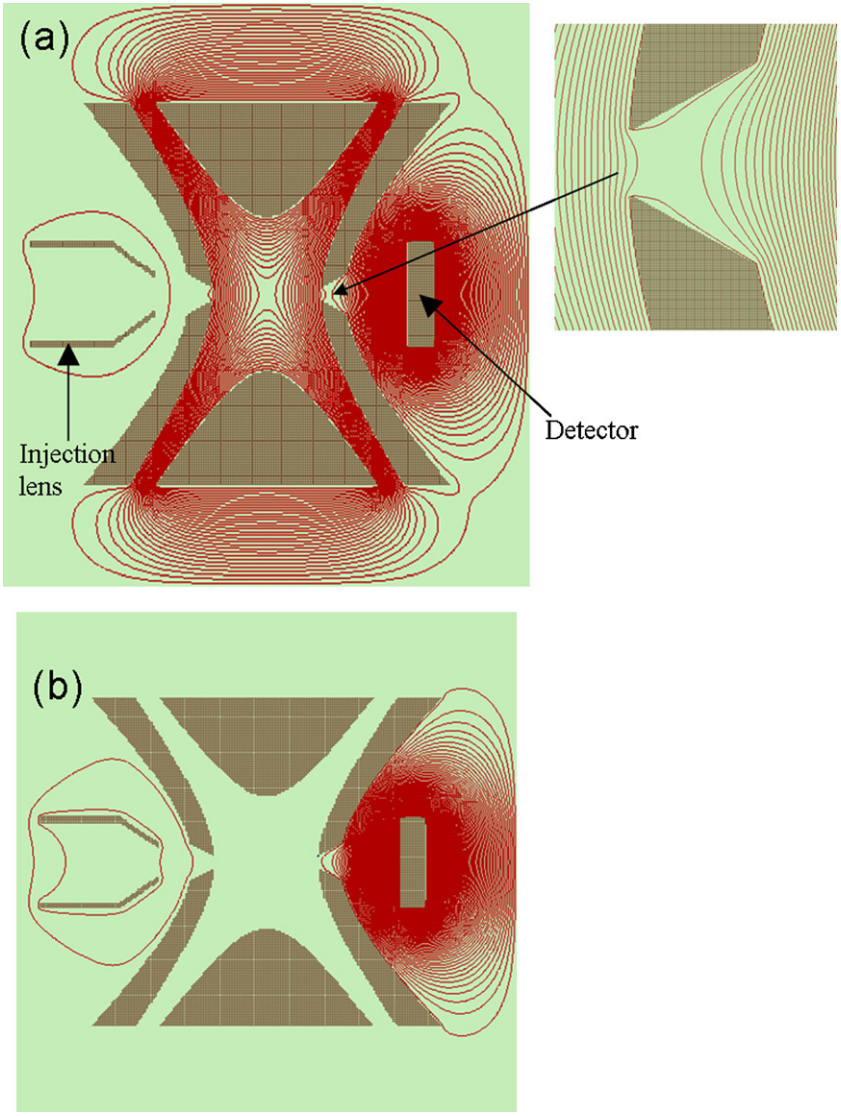

Fig. 1. (a) Geometry and an example of the potential contour plot generated by simulation (SIMION, version 7.0) used to generate the polynomial fit potential along the *z*-axis. (Inset) expanded view of the contour plot at the exit endcap electrode hole. (b) Simulation of the isolated DC potential that arises from the external electrode.

The amplitude dependence on the frequency for the addition of weak octopole field components is given by

$$z^2[(\varepsilon - \kappa_2 z^2)^2 + \lambda^2] = \frac{\hat{f}^2}{4m^2\omega_0^2} \tag{25}$$

Similarly, the amplitude of motion dependence on the frequency with the addition of higher order field components is given by

$$z^2\left[\left(\varepsilon - \sum_i \kappa_i z^i\right)^2 + \lambda^2\right] = \frac{\hat{f}^2}{4m^2\omega_0^2} \tag{26}$$

3. Electric potential

In order to determine the higher order field components inside the nonlinear ion trap, the SIMION version 7 software package was used to numerically model the fields because it allows the field penetration near the endcap hole as well as the truncation effect of having finite electrodes to be determined without the need of deriving complicated analytical expressions. Since the software calculates the fields by the finite difference method, the magnitudes of the small higher order terms inside the nonlinear trap are somewhat dependent on the grid densities. In general, larger grid densities yield better approximations of the small higher order field terms. Unfortunately, larger grid densities require greater computational resources, so there is a tradeoff between computational accuracy and speed. In this study, the goal was to simply demonstrate the effect of negative higher than octopole field components and approximate the effect on the potential due to endcap field penetration. In all cases, the convergence threshold (defined by the SIMION program) was set at 5 μm V per 1000 V for all numerical calculation of the fields.

Multipole field components in a 3D commercial ion trap were reported by Wang and Franzen [20]. More recently, Plass et al. [6] reported higher order field components arise from endcap holes. Similarly, multipole field components were reported for a cylindrical ion trap by several groups [21–23]. In all cases, the fit was performed over the region of space inside the trap using spherical harmonics. Because we are simply interested in the qualitative effect of the negative higher order components that arise from the size of endcap holes, we have simply reported the localized fit along the *z*-axis for illustration. The potential along the *z*-axis was obtained by fitting the numerically derived potential with even

Table 1
The fitting parameters for 4th and 6th order polynomial fits of the potential along the *z*-axis as a function of displacement from the trap center for different endcap holes sizes.

	3.6 mm endcap hole	1.8 mm endcap hole	0.9 mm endcap hole	No endcap hole
f (*only*)	0.22	0.10	−0.029	0.014
f	0.22	0.27	0.17	0.37
g	−0.58	−0.48	−0.25	−0.022

order polynomials of order 4 and 6 by the least squares method. Fitting the potential only along the *z*-axis is justified because resonantly excited ions stay near the *z*-axis during the entire ejection event. The potential was fit to 200 μm away from the electrode surface to minimize the unwanted effects due to finite grid sizes. We also excluded the region where the distance to the plane of the endcap hole was less than 200 μm because pressure differences across the endcap can provide a subtle time averaged "push" when the ions are in this region. This effect is small, but its magnitude increases with mass or cross section. Convergence was observed using over 1 million grid units in the 2D space. Symmetry operations (reflection and rotation) create a 3D grid of well over 6 billion points. Doubling the number of 2D grid points changed the octopole field component by a factor of 1.008 with no change observed for the dodecapole component. Note that these models have grid spacings of 50 and 25 μm with ±25 and ±12.5 μm uncertainty, respectively. The ion trap geometry was defined by rotationally hyperbolic equipotential electrode surfaces characterized by $(r_0/z_0)^2 = 2$. The ideal quadrupole spacing between the electrodes was then increased so that the spacing between the endcap electrodes was "stretched" by 10.6% [24]. This made the trap boundary 7.8 mm from the center. The trap electrodes were truncated at $3r_0$ as in study by Wang and Franzen [20] to minimize field penetration from outside through gaps between electrodes. The trap geometry also included an injection lens and detector electrode. The potential of the injection lens was set to be −15 V and detector surface to be −1 kV relative to average ion trap potential. The entire ion trap was offset with a −10 V potential. The potential inside and outside of the trap is plotted in Fig. 1a with both the lens and detector electrodes energized. The trap is enclosed in a grounded cylinder at the edge of the image in Fig. 1 (not shown). In this study, three different endcap hole sizes were examined and compared to the fields without endcap holes. It is worth pointing out the effect of the small DC component from the external electrodes. The external DC components were isolated from RF and simulated in Fig. 1b. The DC potential due to external electrodes does not significantly affect the potential inside the ion trap. This may be due to the thickness of the endcap electrode near the holes limiting the field penetration from external electrodes. Note also that the external DC components are localized away from the center of the trap. In order to include the minimal effect of the external DC field, a higher order multipole expansion for just the DC part in Eq. (1) is required. An analytical model including a second multipole expansion for the DC part would require a large number of terms and is beyond the scope of this work. Fortunately, the external DC effect is fairly small as shown in Fig. 1b. Its exclusion will not affect any of the results discussed here.

All of the calculated potentials were locally fitted only along the *z*-axis. An example of the fit of the potential along the *z*-axis for 1.8 mm diameter holes is shown in Fig. 2a. The results of the fits are summarized in Table 1. The geometry used in this study was not strictly symmetric because of the outside electrode geometry near the endcap holes. However, our least squares fit with 4th or 6th order polynomials did not show a significant contribution from the odd terms. This observation justifies the use of the simplified equation of motion given above that does not include odd terms.

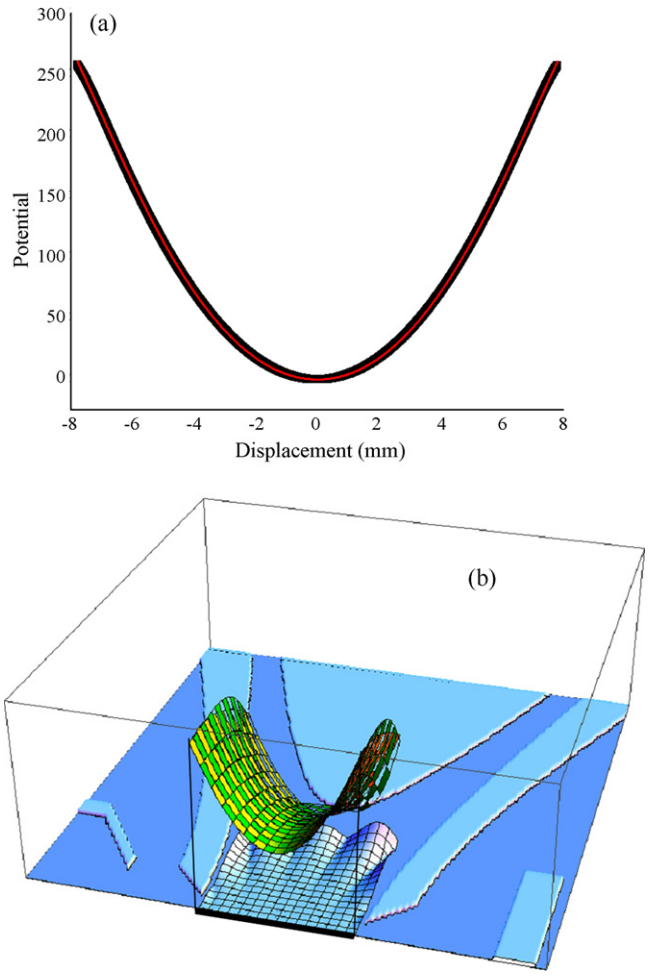

Fig. 2. (a) An example of the fitted potential along the *z*-axis of the ion trap with 1.8 mm diameter endcap holes as a function of displacement from the center. The thick black line represents the points determined by the simulation. The red line indicates the fit of the simulated data with a polynomial that contains up to dodecapole field components. (b) Presents a comparison of the 3D potential generated by plugging our coefficients into a spherical harmonic expansion (green) and the SIMION simulated potential (yellow) for a stretched trap with 1.8 mm endcap holes. The potentials are compared over a 15 mm × 15 mm grid. The multipole expansion coefficients are given in Table 1. Absolute difference between the two potential surfaces is projected on to the light blue mesh at the bottom of the figure. (For interpretation of the references to color in this figure legend, the reader is referred to the web version of the article.)

The octopole and dodecapole field strengths given by $f = A_4/A_2$ and $g = A_6/A_2$, respectively, for four different endcap configurations are summarized in Table 1. Included in Table 1 are the corresponding fits for the three different hole diameters (0.9, 1.8 and 3.6 mm), without endcap holes. Fitting the potential without endcap holes yields very small octopole and dodecapole components in both 4th and 6th order polynomials. The 0.04 octopole component found in 6th order polynomial fit is slightly larger than the value reported by Wang and Franzen [20] where the region of space within trap was fitted by spherical harmonics. Although fitting the 3D volume may provide a better determination of the quadrupole parameter A_2, our calculated value of A_2 (87%) is accurate to within 5%. For this reason, this error will not impact the qualitative results and conclusions reached here. In all cases with the endcap holes, the 6th order polynomial fit shows a significant increase in both the octopole and dodecapole field components and represents a much better fit of the potential near the holes. Interestingly, the 4th order polynomial fit obtained from the potential with 0.9 mm endcap holes shows a negative octopole component. This was due to the error introduced by

local fitting along the z-axis. In the case of a large trap bias and the outer electrode de-energized, both the octopole and dodecapole field components were nearly unchanged.

To examine the effect of our localized fitting of the potential along the z-axis, we have inserted our 6th order fitting coefficients into a spherical harmonic expansion of the 3D potential inside the trap. Fig. 2b shows a comparison of the spherical harmonic expansion of the 3D potential and the SIMION simulated potential of a 10% stretched trap with 1.8 mm endcap holes defined in a 15 mm by 15 mm grid. The comparison between the numerically simulated potential (yellow, Fig. 2b) and our spherical harmonic fit (green, Fig. 2b) up to dodecapole shows an excellent agreement near the z-axis. The deviation between the calculated potential surfaces occurs away from the z-axis near the electrode surfaces. This occurs due to the truncation of the multipole expansion. However, near the center of the trap where the ions remain trapped, the fit is quite good. The regions where the potentials deviate do not make significant contributions to the trajectory of resonantly excited ions. Our 6th order polynomial reliably reproduces the numerically optimized potentials up to very close to the endcap holes. From Table 1,the magnitude of the dodecapole field component along the z-axis steadily increased as the size of the endcap holes was increased over the range studied, whereas the octopole component decreased at a hole diameter of 3.6 mm. The increase of the magnitude of the dodecapole component as the endcap hole size is increased was expected.

4. Results and discussion

The coefficients of the multipole expansion permit calculation of the amplitude response function with higher order field components as a function of endcap hole size. Using Eq. (25) with multipole coefficients up to octopolar field components, the amplitude response curves with octopole field superposition of 0.014, −0.029, 0.10, and 0.22 are shown in Fig. 3. These values were obtained from local fitting along the z-axis with endcap hole diameters of 0 mm (closed), 0.9 mm, 1.8 mm and 3.6 mm, respectively. In all cases in this study, the ion mass-to-charge ratio, buffer gas mass, pressure, secular frequency (ω_0), and excitation voltage are set to 78 amu, 4 amu, 1 mTorr, 100 kHz, and 500 mV unless noted otherwise. All the amplitude response curves show the typical fold over effects. The solid line represents the amplitude response function without holes in the endcap electrodes. This map qualitatively reproduces the results detailed by Makarov [1] and Rajanbabu et al. [11] by showing the same type of fold over. The fold over effect increases in magnitude as the octopole field component increases. Alternatively, negative octopole field components reverse the direction of the fold over (see the dotted line map in Fig. 3).

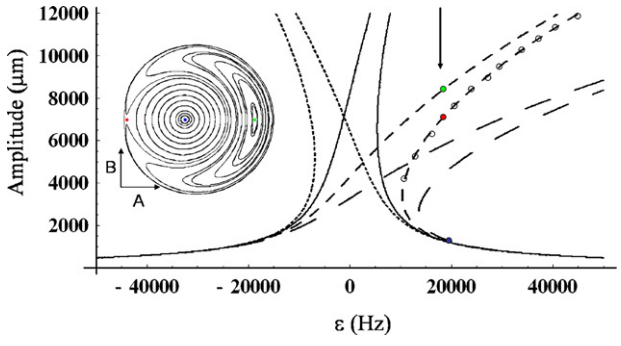

Fig. 3. Amplitude response function generated using up to octopole field components with different sized endcap electrode holes—(solid line) no endcap holes, (dotted line) 0.9 mm holes, (short dash) 1.8 mm holes and (long dash) 3.6 mm diameter holes. The trap boundary is located at 7800 μm. The unstable portions of curves with 1.8 mm endcap holes are illustrated as a group of open circles. The inset is a phase portrait at 20 kHz where the corresponding critical points (indicated by the arrow) are highlighted with corresponding color dots on the amplitude response curve. (For interpretation of the references to color in this figure legend, the reader is referred to the web version of the article.)

Utilization of the "jump condition" for nonlinear ion traps with a positive octopole component has been explained in detail by Makarov [1] and Rajanbabu et al. [11]. Briefly, the forward scan (scanning toward higher mass) can be characterized by moving a point along the curve from the right-hand side of the resonant point at $\varepsilon = 0$ in Fig. 3. The fold over effect increases as the magnitude of the forcing term (excitation voltage) is increased [16]. During the resonant scan, as the ions of a particular mass near resonance, they approach the "jump" point on the amplitude response curve. This is the point where the magnitude of the slope of the amplitude response curve becomes arbitrarily large. At the jump point, the motion of ions with the same m/z becomes coherent and the amplitude "jumps" to the upper surface of the amplitude response function provided the scan speed is slow enough [11]. Therefore, the ions of the same m/z proceed outward as if no-damping gas were present while the ions having a different m/z stay trapped relatively close to the center of the trap [1]. This differentiation can be used to obtain high resolution mass spectra. Without including the presence of holes in the endcap electrodes, only the forward scan can utilize the jump condition. This was used to explain the difference in resolution between forward and reverse scans [1,11]. Note that the upper portion of the lower curve above the jump point was proven to be unstable in this model [25]. Using the same explanation, one may describe the jump condition for the reverse scan for a trap with negative octopole contributions to the field.

However, inclusion of negative higher order terms up to dodecapole using Eq. (26) yields amplitude response curves that are quite different (see Fig. 4). A 1.5 V excitation amplitude was used in the calculation. The amplitude response functions with positive octopole and negative dodecapole field components show three jump points for each map. Note that the expected coalescing of the two separate curves at large amplitude requires the use of a higher order approximation that was not used in this study. Assuming a higher order correction does not change the general shape of the curve, the fourth jump point in Fig. 4 should occur where the two curves are close. For a forward scan, the ions approach the jump point from the right and jump to the same curve. Interestingly, a jump condition also exists in the reverse scan direction when the higher order terms are included. For a reverse scan, the ions approach the jump point from the left. When they meet the jump point, they jump to the other curve in the map to then be ejected from the trap. The reverse scan jump point is located outside (at greater values of oscillation amplitude) of the jump point used in the forward scan. If the experimental parameters are not optimized, the ions may not be ejected as they hop onto the other curve. In this

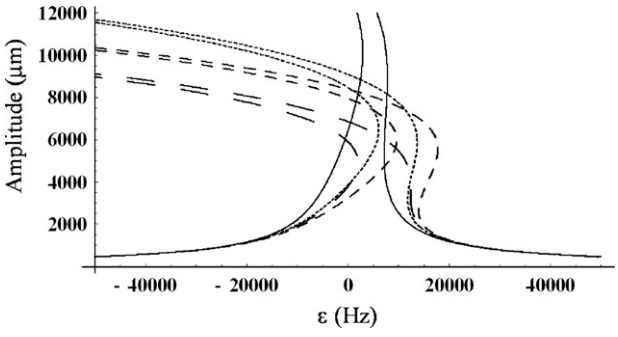

Fig. 4. Amplitude response function generated using up to dodecapole field components with different sized endcap electrode holes—(solid line) no endcap holes, (dotted line) 0.9 mm holes, (short dash) 1.8 mm holes and (long dash) 3.6 mm diameter holes. Dipole excitation voltage = 1.5 V. The trap boundary is located at 7800 μm.

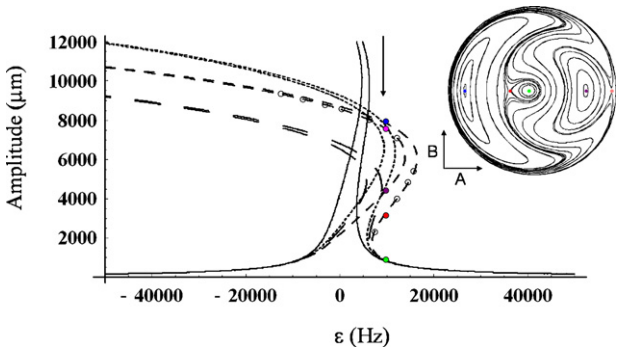

Fig. 5. Amplitude response function generated using up to dodecapole field components with different sized endcap electrode holes—(solid line) no endcap holes, (dotted line) 0.9 mm holes, (short dash) 1.8 mm holes and (long dash) 3.6 mm diameter holes. Dipole excitation voltage = 0.5 V The unstable portion of curves with 1.8 mm endcap holes are illustrated as a group of open circles. The inset is a phase portrait at 8 kHz where the corresponding critical points (indicated by the arrow) are highlighted with corresponding color dots on amplitude response curve. The trap boundary is located at 7800 μm. (For interpretation of the references to color in this figure legend, the reader is referred to the web version of the article.)

case, the ions would shrink toward the center of the trap as they proceed to the right-hand side of resonance point.

Inspection of the amplitude response functions in Fig. 4 suggests some interesting possibilities for future experiments. The amplitude response function has a continuous parametric dependence on the size of the endcap holes. The shape of the amplitude response functions also depends on the forcing and damping terms. In Fig. 5, the voltage of the dipole excitation applied to the endcap electrodes (the forcing term) was changed to 500 mV. In this case, the curves overlap over a short range of values of the detuning parameter, ε. Under the conditions in Fig. 5, where the curves overlap, the ions will not be ejected from the trap because the upper curve surface is not outside the trap boundary at $z = 7800$ μm. Crossing to the other curve will occur and the ions will then de-excite and return to the center of the trap. It may be feasible to construct a trap and find a set of conditions where the jump points from either scan direction overlap at the same detuning parameter with ejection from the trap. When the two jump points coincide, the mass of ions measured in both scan directions will coincide if the scan speed is slow enough. The effect that overlapping the jump points has on resolution could also be experimentally interesting.

Using the multiple scale analysis described in Appendix A, the stability of the stationary states was characterized in this study. Also illustrated as an inset in Figs. 3 and 5 are phase portraits at selected values of ε of 20 and 8 kHz (indicated by the arrows in the figures), respectively. The phase portraits were generated using a set of closed trajectories by numerical integration of the autonomous equations under no-damping conditions. The portrait in Fig. 3 produced three critical points. Two of the critical points, shown as blue and green dots, are spiral sinks. Under damping conditions, trajectories near those points will travel spiral paths and eventually settle at those points thereby indicating their stability. The red dot in the phase portrait of Fig. 3 represents a saddle point, where trajectories are unstable and will move away from that point. The corresponding critical points associated with the selected value of $\varepsilon = 20$ kHz are shown as colored dots on the amplitude response curves. A group of saddle points, indicated as open circles in Fig. 3, illustrate that the underside of the curve from the jump point on is unstable. The phase portrait in Fig. 5 produced five critical points. Three of the points illustrated as green, purple and blue dots are spiral sinks. Two of the critical points are saddle points. The group of open circles indicates the region of the amplitude response curves that are unstable saddle points. These results show that the unstable portions of the curve are again on the undersides of the curves after (or between) the jump points. The lowest portion of both curves is asymptotically stable in the presence of damping gas. Therefore, ions start out very close to the trap center before they experience resonance excitation. The lower portions of the curves are stable until a jump point is reached. Therefore, no jump is allowed before the jump point in both forward and reverse scans. When the amplitude response curve exhibits four distinct jump points (assuming that the curves coalesce), up to five distinct steady state solutions are possible at a particular frequency.

To obtain a more accurate description of ion motion in nonlinear ion traps, even higher order potential components of the field may be required to allow a better description of ion motion. Unfortunately, the model will become more complex and difficult to solve numerically. However, inclusion of the dodecapole term used in this model provided a good initial step for modeling the effect of field penetration through the endcap holes.

5. Conclusions

The effect of negative higher order field components induced by the presence of holes in the endcap electrodes on the resonance ejection of ions from a trap has been explored. These results suggest that jump conditions exist in both the forward and reverse scan modes when the effects of the endcap holes are considered. The presence of the holes has interesting implications for the ejection processes that are observed in ion traps during resonance ejection. They produce a jump condition in the reverse scan direction. The shape of the response function was shown to be dependent on the trap geometry (including holes) and the operating conditions. Optimization of the response function shape presents interesting possibilities that warrant further investigation in terms of mass resolution.

Acknowledgements

We wish to thank the anonymous reviewers for their insightful comments. This research was funded by the US Department of Energy, Office of Nonproliferation Research and Engineering under Contract No. DE-AC05-00OR22725 with Oak Ridge National Laboratory, managed and operated by UT-Battelle, LLC.

Appendix A

A.1. Stability of the stationary solutions of double jump amplitude plot

Although it was convenient to construct amplitude response curves from the implicit relation, this approach does not give insight into the stability of stationary states. It is important to distinguish the stability of the states because the trajectory depends greatly on the types of critical points present. The simplest approach to find the nature of critical points is to use methods of multiple scales [26]. Rajanbabu et al. [11] used this method for weak octopole systems. Using the same approach to account for the field penetration through the endcap hole, the nonlinear potential was expanded to the dodecapole term where its component is negative.

After multiple variable transformations described in Rajanbabu et al. [11], our equation of motion becomes

$$\frac{d^2\tilde{z}}{d\tau^2} + \upsilon^2\tilde{z} = \varepsilon\left(\delta\tilde{z} - 2\mu\frac{d\tilde{z}}{d\tau} - \tilde{\beta}\tilde{z}^3 - \tilde{\eta}\tilde{z}^5 + F\cos\nu\tau\right)$$

where

$$\tau = \omega_0 t, \quad \upsilon = \frac{\gamma}{\omega_0}, \quad \tilde{z} = \frac{z}{r_0}, \quad \nu^2 = 1 + \varepsilon\delta, \quad F = \frac{\hat{f}}{m\omega_0^2 r_0}, \quad \tilde{\beta} = 8f,$$

and $\tilde{\eta} = 9g$

To separate the slow and fast motions, two ranges of time scale were used:

$$T_0 = \tau, \quad T_1 = \varepsilon\tau$$

The solution of the equation of motion was expanded to

$$\tilde{z}(T_0, T_1) = Z_0(T_0, T_1) + \varepsilon Z_1(T_0, T_1)$$

where Z_0 has the general solution of the form

$$Z_0 = A(T_1)\cos(\upsilon\tau) + B(T_1)\sin(\upsilon\tau)$$

Derivatives with respect to τ are given by the chain rule

$$\frac{d}{d\tau} = \frac{\partial}{\partial T_0} + \varepsilon\frac{\partial}{\partial T_1}, \quad \frac{d^2}{d\tau^2} = \frac{\partial^2}{\partial T_0^2} + 2\varepsilon\frac{\partial^2}{\partial T_0 \partial T_1}$$

After substituting the last two equations into the equation of motion, gathering the vanishing secular term and then setting $\varepsilon = 1$, we obtained the autonomous equations:

$$\frac{dA}{d\tau} = \frac{1}{8\upsilon}\left(-8\mu\upsilon A - 4\delta B + 3\tilde{\beta}A^2B + 3\tilde{\beta}B^3 + \frac{5}{2}\tilde{\eta}A^4B + 5\tilde{\eta}A^2B^3 + \frac{5}{2}\tilde{\eta}B^5\right)$$

$$\frac{dB}{d\tau} = \frac{1}{8\upsilon}\left(-8\mu\upsilon B + 4\delta A - 3\tilde{\beta}AB^2 - 3\tilde{\beta}A^3 - \frac{5}{2}\tilde{\eta}AB^4 - 5\tilde{\eta}A^3B^2 - \frac{5}{2}\tilde{\eta}A^5 + 4F\right)$$

In order to investigate the nature of critical points, these equations were linearized to

$$\Theta'\begin{pmatrix} A \\ B \end{pmatrix} = J\Theta\begin{pmatrix} A \\ B \end{pmatrix}$$

where J is the Jacobian matrix,

$$J = \frac{1}{8\upsilon}\begin{bmatrix} J_{11} & J_{12} \\ J_{21} & J_{22} \end{bmatrix}$$

$$J_{11} = -8\mu\upsilon + 6\tilde{\beta}AB + 10\tilde{\eta}A^3B + 5\tilde{\eta}AB^3$$

$$J_{12} = -4\delta + 3\tilde{\beta}A^2 + 9\tilde{\beta}B^2 + \frac{5}{2}\tilde{\eta}A^4 + 15\tilde{\eta}A^2B^2 + \frac{25}{2}\tilde{\eta}B^4$$

$$J_{21} = 4\delta - 9\tilde{\beta}A^2 - 3\tilde{\beta}B^2 - \frac{5}{2}\tilde{\eta}B^4 - 15\tilde{\eta}A^2B^2 + \frac{25}{2}\tilde{\eta}A^4$$

$$J_{11} = -8\mu\upsilon - 6\tilde{\beta}AB - 5\tilde{\eta}A^3B - 10\tilde{\eta}AB^3$$

Using this linearized equation, the critical points on the amplitude response curves were investigated in terms of their stability.

References

[1] A.A. Makarov, Anal. Chem. 68 (1996) 4257.
[2] J.D. Williams, K.A. Cox, R.G. Cooks, R.E. Kaiser, J.C. Schwartz, Rapid Commun. Mass Spectrom. 5 (1991) 327.
[3] N.S. Arnold, G. Hars, H.L.C. Meuzelaar, J. Am. Soc. Mass Spectrom. 5 (1994) 676.
[4] F.A. Londry, G.J. Wells, R.E. March, Rapid Commun. Mass Spectrom. 7 (1993) 43.
[5] J.M. Wells, W.R. Plass, G.E. Patterson, O.Y. Zheng, E.R. Badman, R.G. Cooks, Anal. Chem. 71 (1999) 3405.
[6] W.R. Plass, H.Y. Li, R.G. Cooks, Int. J. Mass Spectrom. 228 (2003) 237.
[7] L. Ding, M. Sudakov, S. Kumashiro, Int. J. Mass Spectrom. 221 (2002) 117.
[8] L. Ding, M. Sudakov, F.L. Brancia, R. Giles, S. Kumashiro, J. Mass Spectrom. 39 (2004) 471.
[9] S. Sevugarajan, A.G. Menon, Int. J. Mass Spectrom. 209 (2001) 209.
[10] G.T. Abraham, A. Chatterjee, A.G. Menon, Int. J. Mass Spectrom. 231 (2004) 1.
[11] N. Rajanbabu, A. Chatterjee, A.G. Menon, Int. J. Mass Spectrom. 261 (2007) 159.
[12] J. Yoda, K. Sugiyama, Jpn. J. Appl. Phys. Part 1: Regular Papers Short Notes & Review Papers 31 (1992) 3744.
[13] X. Luo, X. Zhu, K. Gao, J. Li, M. Yan, L. Shi, J. Xu, Appl. Phys. B: Lasers Opt. 62 (1996) 421.
[14] S. Sevugarajan, A.G. Menon, Int. J. Mass Spectrom. 189 (1999) 53.
[15] S. Sevugarajan, A.G. Menon, Int. J. Mass Spectrom. 197 (2000) 263.
[16] L.D. Landau, E.M. Lifshitz, Mechanics, 3rd ed., Butterworth-Heinemann, 1982.
[17] A.L. Michaud, A.J. Frank, C. Ding, X.Z. Zhao, D.J. Douglas, J. Am. Soc. Mass Spectrom. 16 (2005) 835.
[18] J.B. Marion, S.T. Thorton, Classical Dynamics of Particles and Systems, 4th ed., Harcourt, New York, 1995, p. 638.
[19] C. Knight, W.D. Ruderman, M.A. Helmholz, C.A. Moyer, B.J. Kittel, Mechanics: Berkeley Physics Course, vol. 1, McGraw-Hill, 1965.
[20] Y. Wang, J. Franzen, Int. J. Mass Spectrom. Ion Process. 132 (1994) 155.
[21] O. Kornienko, P.T.A. Reilly, W.B. Whitten, J.M. Ramsey, Rapid Commun. Mass Spectrom. 13 (1999) 50.
[22] G.X. Wu, R.G. Cooks, Z. Ouyang, Int. J. Mass Spectrom. 241 (2005) 119.
[23] P.K. Tallapragada, A.K. Mohanty, A. Chatterjee, A.G. Menon, Int. J. Mass Spectrom. 264 (2007) 38.
[24] R.E. March, J.F.J. Todd, Practical Aspects of Ion Trap Mass Spectrometry: Fundamentals, vol. 1, CRC Press, Boca Raton, FL, 1995, p. 430.
[25] Y.A. Mitropol'skii, Problems of the Asymptotic Theory of Non-Stationary Vibrations, Israel Program for Scientific Translations, Jerusalem, 1965.
[26] A.H. Nayfeh, Perturbation Methods, Wiley Interscience Publications, New York, 1973.